

RESEARCH ARTICLE

10.1002/2016JD025855

Key Points:

- VPD has increased in the past and will continue to increase in the future
- Increases in VPD are driven by increases in saturation vapor pressure and declines or small changes in actual vapor pressure
- Future increases in VPD are expected to reduce stomatal conductance by 9–51%

Supporting Information:

- Supporting Information S1

Correspondence to:

D. L. Ficklin,
dficklin@indiana.edu

Citation:

Ficklin, D. L., and K. A. Novick (2017), Historic and projected changes in vapor pressure deficit suggest a continental-scale drying of the United States atmosphere, *J. Geophys. Res. Atmos.*, *122*, 2061–2079, doi:10.1002/2016JD025855.

Received 30 AUG 2016

Accepted 24 DEC 2016

Accepted article online 2 FEB 2017

Published online 16 FEB 2017

Historic and projected changes in vapor pressure deficit suggest a continental-scale drying of the United States atmosphere

Darren L. Ficklin¹  and Kimberly A. Novick² 

¹Department of Geography, Indiana University Bloomington, Bloomington, Indiana, USA, ²School of Public and Environmental Affairs, Indiana University Bloomington, Bloomington, Indiana, USA

Abstract Via air temperature increases and relative humidity changes, climate change will modify vapor pressure deficit (VPD), which is an important determinant of water vapor and CO₂ exchange between the land surface and atmosphere. VPD is the difference between the water vapor the air can hold at saturation (e_s) and the actual amount of water vapor (e_a). Here we assess changes in VPD, e_s , and e_a in the United States (U.S.) for the recent past (1979–2013) and the future (2065–2099) using gridded, observed climate data and output from general circulation models. Historically, VPD has increased for all seasons, driven by increases in e_s and declines in e_a . The spring, summer, and fall seasons exhibited the largest areal extent of significant increases in VPD, which was largely concentrated in the western and southern portions of the U.S. The changes in VPD stemmed from recent air temperature increases and relative humidity decreases. Projections indicate similar, amplified patterns into the future. For the summer, the general circulation model ensemble median showed a 51% projected increase (quartile range of 39 and 64%) in summer VPD for the U.S., reflecting temperature-driven increases in e_s but decreases or minimal changes in relative humidity that promotes negligible changes in e_a . Using a simple model for plant hydraulic functioning, we also show that in the absence of stomatal acclimation, future changes in VPD can reduce stomatal conductance by 9–51%, which is a magnitude comparable to the expected decline in stomatal conductance from rising CO₂.

1. Introduction

Global air temperature has increased by at least 0.2°C per decade over the last 30 years [Hartmann *et al.*, 2013]. Based on the Clausius-Clapeyron relationship, increased air temperature leads to higher-saturation water vapor pressure (e_s), defined as amount of water vapor the air can hold at saturation [Bohren *et al.*, 2000; Breshears *et al.*, 2013]; as a result, global temperature-driven increases in e_s have been reported in many studies [Isaac and van Wijngaarden, 2012; Kunkel *et al.*, 2013; Lobell *et al.*, 2013; Seager *et al.*, 2015]. Actual water vapor pressure (e_a) is determined by a larger number of drivers. It is also related to air temperature due to the fact that, on the upper end, e_a is constrained by e_s . Thus, the warmer the air, the larger the maximum amount of water vapor. However, e_a is also dependent on the amount of moisture in the air, which in turn is linked to the hydrologic cycle and regional to global scale circulation patterns. Therefore, decreases in humidity, driven, for example, by continental-scale circulations or limitations to evapotranspiration imposed by low soil moisture availability or reduced stomatal conductance, can prevent e_a from increasing as quickly as e_s as temperatures rise.

The difference between e_s and e_a is the vapor pressure deficit (VPD), which is the measure of atmospheric desiccation strength [Seager *et al.*, 2015] and is an important determinant of the atmospheric demand for water vapor. While e_s is always greater than or equal to e_a (unless the environment is supersaturated), the difference between the two can be highly variable. Because e_s is driven solely by temperature, it is expected to increase with future air temperature increases. The future relationship of e_s to e_a (and therefore VPD) is still uncertain, and will reflect the extent the limitation of water movement from the land surface to the atmosphere by the future climate.

VPD is a critical driver of ecosystem function. It is directly related to evapotranspiration (ET), and over nonvegetated or sparsely vegetated surfaces an increase in VPD will promote an increase in ET, which can affect soil moisture and precipitation dynamics. It is widely known, however, that plant stomatal conductance (g_s) is inversely related to VPD [Cowan and Farquhar, 1977; McAdam and Brodrigg, 2015; McDowell and Allen,

2015; Oren *et al.*, 1999; Whitehead, 1998], reflecting the fact that stomates close to prevent excessive water loss in a desiccating atmosphere. Because the relationship between ET and g_s is hyperbolic (at least when conceptualized using the Penman-Monteith equation [Penman, 1948; Monteith, 1965]), declines in g_s with increasing VPD reduce ET from its potential rate. Declines in stomatal conductance with rising VPD represent a significant constraint on plant carbon uptake and productivity [Eamus *et al.*, 2013; Lasslop *et al.*, 2010; McDowell and Allen, 2015], though these limitations may be buffered by changes in water use efficiency with rising CO₂ [Ainsworth and Rogers, 2007; Katul *et al.*, 2009; Medlyn *et al.*, 2011]. Other studies have demonstrated that VPD is correlated to wild fire incidence [Seager *et al.*, 2015; Williams *et al.*, 2014] and has a larger relationship to forest/grassland fire than several other factors such as precipitation, drought indices, temperature, and wind [Williams *et al.*, 2015]. Due to its close connection to ecosystem carbon cycling and disturbance events, VPD has also been identified as a critical determinant of tree mortality [Williams *et al.*, 2015].

While the importance of VPD on ecosystem productivity, water cycling, and mortality is well-established, historical and projected changes in VPD (including e_s and e_a) are not as well understood. Previous work has concluded that VPD did not change appreciably during the second half of the twentieth century [Roderick and Farquhar, 2002]. Other works highlight evidence for, or an assumption of, constant global relative humidity as climate change proceeds [Dessler and Sherwood, 2009; Willett *et al.*, 2007], which implies increases in VPD that are consistent with global patterns of temperature rise. The assumption of constant VPD with a changing climate is inconsistent with work by Seager *et al.* [2015] showing that trends in VPD, e_s , and e_a between 1960 and 2013 are spatially and temporally variable for the United States, and recent work by Zhang *et al.* [2015] showing an overall increase in global atmospheric moisture demand (0.75 mm/yr) from 1988 to 2008. Using general circulation models (GCMs), Smith *et al.* [2016] show a projected global increase in VPD, and Williams *et al.* [2013] show a projected increase in VPD for the southwestern United States.

Spatially explicit presentations of historic and future trends in VPD are furthermore difficult to find in the literature. While several studies include maps of historic and/or future changes in relative humidity [Lainé *et al.*, 2014; Fu and Feng, 2014; Seager *et al.*, 2015; Byrne and O'Gorman, 2016], maps of historic and future changes in VPD are largely absent from the literature. Relative humidity and VPD are correlated but not linearly related, and they do not identically affect plant functioning [Leuning, 1995; Sato *et al.*, 2015]. To our knowledge, this study will be among the first to provide spatially explicit representations of historic and future changes in VPD for the continental United States, and furthermore to leverage those data into spatially explicit predictions for how trends in VPD may affect stomatal conductance independently of responses to other hydroclimatic variables (i.e., elevated CO₂, soil moisture, and radiation).

Here we build on previous studies of VPD trends by using high-resolution climate data from 1979 to 2013 to assess recent trends in VPD, e_s , e_a , and contributing climatic components. Additionally, we assess how VPD, e_s , and e_a might change in the future through the use of 18 downscaled GCMs. Finally, to begin to understand the implications of these trends in VPD for ecosystem functioning, we use concepts from plant hydraulic theory to provide an estimate on the reductions in stomatal conductance attributable to past and historic patterns in VPD.

2. Materials and Methods

2.1. Climate Data

Gridded (4 km resolution) historical daily climate data (aggregated to monthly data), including maximum and minimum temperature and specific humidity, for the years 1979–2013 were extracted from the University of Idaho Gridded Surface Meteorological Data data set (METDATA) [Abatzoglou, 2013]. METDATA is a combination of temporally rich North American Land Data Assimilation System-Phase 2 (NLDAS-2) [Mitchell *et al.*, 2004] and spatially rich Parameter-elevation Regressions on Independent Slopes Model (PRISM) [Daly *et al.*, 2008]. Validation of METDATA against observations indicates skill comparable to direct interpolation from observations, especially for air temperature and relative humidity, the variables used for this work. Correlations between METDATA and observations for maximum and minimum air temperature for the western United States were 0.94 and 0.87, respectively, while correlations were 0.77 and 0.81 for maximum and minimum relative humidity, respectively [Abatzoglou, 2013]. We therefore have full confidence that the observational data set is accurate in its representation of air temperature and relative humidity throughout the United States. Full details of this data set are available at <http://metdata.northwestknowledge.net/>.

Additionally, downscaled output from 18 GCMs participating in the fifth Coupled Model Intercomparison Project (CMIP5) that had monthly output of maximum and minimum temperature and specific humidity were extracted for Representative Concentration Pathway 8.5 (highest-emission pathway) for the 1950–2099 time period (Table S1 in the supporting information). Bias correction and statistical downscaling of these variables for all models were performed using the Multivariate Adaptive Constructed Analogs approach (MACA version 2) [Abatzoglou and Brown, 2012] to the reference 4 km METDATA data set [Abatzoglou, 2013]. The bias-corrected/downscaled GCM data can be obtained at <http://maca.northwestknowledge.net/>. The acronyms shown in the supporting information figures are fully explained on the previously mentioned website and in Table S1.

In order to present high spatial resolution projections of VPD and its underlying components, downscaling must be performed. GCM output is on the order of $\sim 150\text{--}300\text{ km}^2 \times \sim 150\text{--}300\text{ km}^2$, a resolution much too coarse than any hydrological/ecohydrological (i.e., watershed or forest) application. This is especially true for topographically complex areas where temperature, for example, can vary tremendously within 10 to 20 km. Some type of downscaling must be performed in order to translate original GCM output to a local or regional scale needed for impact studies. There are numerous techniques to translate low-resolution GCM output to the high-resolution projections [Fowler *et al.*, 2007], though this is not the topic of the present study.

In this study the GCM data were downscaled to the METDATA gridded, observational data set (also used in this study) using the MACA method developed by Abatzoglou and Brown [2012]. This method (and all statistical downscaling techniques) assumes that the large-scale meteorology from GCMs are related (statistically) to the meteorology at local scales (at climate stations, for example). It is also important to note that the statistical downscaling methods also assume stationarity (i.e., the statistical relationships that hold true in the present may not hold true in the future). The MACA method uses a combination of quantile mapping and constructed analogs, which jointly find target patterns for maximum and minimum air temperature and dew point temperature and is fully described in Abatzoglou and Brown [2012]. The MACA method exhibited great skill in temperature and humidity (the variables used in this work) for the complex topography of the western United States [Abatzoglou and Brown, 2012]. Additionally, the MACA approach was further adjusted to ensure the preservation of trends from raw GCM output to downscaled fields at monthly timescales [Pierce *et al.*, 2015]. We therefore have full confidence that the downscaled GCM data used in this work are physically plausible projections of VPD and its underlying components.

The downscaled data used in this study are also bias corrected within the MACA approach. Previous work has documented GCM biases in simulating regional climate [e.g., Maurer and Hidalgo, 2008; Polade *et al.*, 2013; Rupp *et al.*, 2013; Ficklin *et al.*, 2016a], which include differences in the magnitude, seasonality, and variability of GCM output relative to observations and should translate into similar biases in projections. These biases can also propagate into regional climate model (RCM) output if used for dynamic downscaling [Racherla *et al.*, 2012]. At the local scale, such biases can substantially alter annual moisture related variables [e.g., Johnson and Sharma, 2010; Maurer and Pierce, 2014]. Previous work [Ficklin *et al.*, 2016a] shows that the GCM biases do matter when assessing future changes in aridity and drought.

One thing to note is that the observed climate data (METDATA) includes the influence of irrigation on regional climate while the projected climate data (MACA) does not. Previous work indicates that irrigation can have a localized cooling effect on air temperature from increased cloud cover and increase precipitation downwind of irrigated areas [Sacks *et al.*, 2009; Puma and Cook, 2010].

2.2. Estimation of Vapor Pressure Deficit, Saturation Vapor Pressure, and Actual Vapor Pressure

VPD, e_s , and e_a were estimated using the approach of Allen *et al.* [1998] for every grid point of the METDATA and MACA data sets. Specifically, e_s (kPa) was calculated by

$$e_{s, \min} = 0.611 \times \exp\left(\frac{17.3 \times T_{\min}}{T_{\min} + 237.3}\right) \quad (1)$$

$$e_{s, \max} = 0.611 \times \exp\left(\frac{17.3 \times T_{\max}}{T_{\max} + 237.3}\right) \quad (2)$$

$$e_s = 0.5 \times (e_{s, \min} + e_{s, \max}) \quad (3)$$

where T_{\min} and $e_{s,\min}$, and T_{\max} and $e_{s,\max}$ are the minimum and maximum temperatures ($^{\circ}\text{C}$) and saturation vapor pressures (kPa), respectively. The e_a (kPa) was calculated by

$$e_a = \text{RH} \times \frac{e_s}{100} \quad (4)$$

where RH is relative humidity (%) and is estimated by

$$\text{RH} = 100 \times \frac{(\text{SH} \times \rho)}{(e_s \times 0.622)} \quad (5)$$

where SH is specific humidity (kg/kg) extracted from either METDATA or MACA, and ρ is the atmospheric pressure corrected for elevation (kPa), which is estimated by

$$\rho = \rho_{\text{sea level}} \times \frac{(293 - 0.0065 \times \text{elevation})^{5.26}}{293} \quad (6)$$

where $\rho_{\text{sea level}}$ is the pressure at sea level (101.3 kPa) and elevation is the elevation (m) above sea level for the particular grid point. Finally, VPD (kPa) is estimated by

$$\text{VPD} = e_s - e_a \quad (7)$$

When linking results from this work to plant functioning, it is important to note that our estimates of VPD represent daily averages (aggregated to a monthly time step) that consider both daytime and nocturnal values. Since vegetation photosynthesizes during the day, one would expect that daytime VPD would be the most relevant driver for plant ecosystem productivity, water cycling, and mortality. The averaging of maximum and minimum e_s treats daytime atmospheric conditions equal to nighttime atmospheric conditions, which will lower VPD. Therefore, for plant-specific effects from increases in VPD, the results from this study should be viewed as conservative.

2.3. Estimation of Projected Stomatal Functioning

Darcy's law states that the flux of water from the soil to the leaves (T_r) may be described via an Ohm's law analogy [van den Honert, 1948]:

$$T_r = K(\Psi_S - \Psi_L - \rho gh) \quad (8)$$

where K is the whole-plant hydraulic conductance, Ψ_S and Ψ_L are the leaf and soil water potentials, respectively, and the term ρgh accounts for gravity induced head losses. Under steady state conditions characterized by low boundary layer resistance and little hydraulic capacitance, T_r may be equated to the product of stomatal conductance (g_s) and VPD [Whitehead, 1998], giving

$$g_s = \frac{[K(\Psi_S - \Psi_L - \rho gh)]}{\text{VPD}} \quad (9)$$

The term in the numerator reflects a wide variety of biophysical properties, including xylem anatomy, canopy structure, species-specific regulation of leaf water potential (i.e., isohydric versus anisohydric), and soil moisture content. Here we make a simplifying but limiting assumption that the term $T_r = K(\Psi_S - \Psi_L - \rho gh)$ is invariant with VPD, which allows us to straightforwardly determine the relative change in g_s imposed by variation in VPD between two time periods (time1, time2) as

$$\text{Relative } g_s = \frac{g_{s,\text{time2}} - g_{s,\text{time1}}}{g_{s,\text{time1}}} = \frac{\left(\frac{1}{\text{VPD}_{\text{time2}}} - \frac{1}{\text{VPD}_{\text{time1}}}\right)}{\frac{1}{\text{VPD}_{\text{time1}}}} \times 100 \quad (10)$$

Using equation (10), we then estimate the expected magnitude of the change in g_s (as percent change) driven by nonstationary VPD in the absence of changes in other biophysical variables.

We stress that, in reality, the biophysical determinants of $K(\Psi_S - \Psi_L - \rho gh)$ are indeed likely to change over long time scales, in ways that are independent of changes in g_s imposed by rising VPD. For example, future changes in VPD may also be accompanied by future changes in soil water potential. In general, future

projections of changes in soil moisture content are spatially heterogeneous but tend to represent temporal decreases over time [Jung et al., 2010; Laine et al., 2014]. Thus, we consider another estimate of relative g_s that is representative of a ~20% decline in soil moisture content between future and present conditions. This assumed decline is consistent with model predictions for some terrestrial ecosystems [Sheffield and Wood, 2008] and is also similar to the mean decline in growing season soil moisture content observed during some naturally occurring drought events [Stoy et al., 2006]. Because the relationship between soil water potential and soil moisture content is nonlinear [Clapp and Hornberger, 1978], a 20% decline in soil moisture results in decline in soil water potential that varies depending on soil type and normal soil moisture conditions. For example, using the model of Clapp and Hornberger [1978], a 20% decline in soil moisture content in a silt loam that is 70% saturated is on the order of 0.1 MPa; a similar decline in a sandy loam that is 40% saturated is on the order of ~0.4 MPa. For the purposes of this simple exercise, we assume a decline in Ψ_S of -0.3 MPa. During normal, nondrought periods, $(\Psi_S - \Psi_L - \rho gh) = 1.0$ MPa is a reasonable approximation for many tree species [Roman et al., 2015], so that a 0.3 MPa decline in Ψ_S translates to a 30% reduction in $(\Psi_S - \Psi_L - \rho gh)$. Thus, another estimate of relative g_s that reflects temporal declines in soil moisture ($g_{s,SM \downarrow}$) may be calculated from

$$\text{Relative } g_{s,SM \downarrow} = \frac{g_{s,time2} - g_{s,time1}}{g_{s,time1}} = \frac{\left(\frac{0.7}{VPD_{time2}} - \frac{1}{VPD_{time1}}\right)}{\frac{1}{VPD_{time1}}} \times 100 \quad (11)$$

Similarly, we also produced an estimate of relative g_s that accommodates the potential for adaptive increases in the quantity $K(\Psi_S - \Psi_L - \rho gh)$. These adaptations could represent increases in whole-plant hydraulic conductivity K , achieved, for example, by increases in the sapwood area, declines in the leaf area, or declines in plant height [McDowell et al., 2002; Novick et al., 2009]. They could also represent increases in the difference between soil and leaf water potential driven by more anisohydric (i.e., risky) hydraulic regulation [McDowell et al., 2002; Roman et al., 2015]. It is important to note that any of these adaptive strategies could have a negative impact on carbon assimilation or growth, for example, by requiring a tree to invest in additional sapwood area instead of additional height, or by increasing the risk of damaging hydraulic cavitation. Nonetheless, for the purposes of this study, we consider the case of a 30% increase in $K(\Psi_S - \Psi_L - \rho gh)$ between present and future climate conditions. This assumed magnitude is consistent with observed height-driven adaptive changes in the plant sapwood-to-leaf area ratio as a tree matures from a sapling to a mature adult [McDowell et al., 2002; Novick et al., 2009], though it could also represent increasingly anisohydric behavior in the future. With this assumption, a final estimate of relative g_s that reflects hydraulic adaptation ($g_{s,adaptive}$) may be calculated from

$$\text{Relative } g_{s,adaptive} = \frac{g_{s,time2} - g_{s,time1}}{g_{s,time1}} = \frac{\left(\frac{1.3}{VPD_{time2}} - \frac{1}{VPD_{time1}}\right)}{\frac{1}{VPD_{time1}}} \times 100 \quad (12)$$

2.4. Statistical Analyses

Statistical analyses and trends of VPD, e_s , and e_a and their climatic components were performed for the period from 1979 to 2013 (defined as historical) for the METDATA and the period from 2065 to 2099 for the MACA (defined as projected). As with any trend test, the start and the end points of the time series affect the trend magnitude and/or direction. For example, a trend test on a time series starting in January 1979 and ending in December 2000 will very likely give different results than a time series starting in January 1979 and ending in December 2013. The monthly data were broken up into seasons: winter (December, January, February; DJF), spring (March, April, May; MAM), summer (June, July, August; JJA), and fall (September, October, November; SON). Months within a season were then averaged for each year. Trends and their statistical significance for the historical time period were assessed using two trend metrics: Sen-Theil slope estimator [Sen, 1968; Theil, 1992] for the trend magnitude and the Mann-Kendall trend test [Kendall, 1975; Mann, 1945] for the trend significance at $p < 0.05$. Using the Mann-Kendall test requires serially independent data, otherwise the trend significance will be overestimated [Yue et al., 2002]. We find that serial correlation is not a concern for the seasonal data used in this work. After the first lag, correlation decreases from 1 (0 lag) to a range of 0.0 to 0.2 for all climate variables for the United States.

To assess projected changes in VPD, e_s , e_a , and their underlying climatic components, the difference between the historical and projected time periods of individual GCMs were calculated. Using the GCM ensemble, the median, first, and third quartiles were calculated. Previous work has found that spurious trends can be found when climate stations with different statistical distributions go offline or online throughout the time of gridded data generation [Hamlet and Lettenmaier, 2005; Livneh et al., 2013; Maurer et al., 2002], though the use of METDATA (a combination of PRISM and NLDAS-2) should alleviate these concerns.

3. Results and Discussion

3.1. Historical Trends in Vapor Pressure Deficit, Saturation Vapor Pressure, and Actual Vapor Pressure

Statistically significant trends of VPD were observed during the historical time period (1979–2013) for all seasons. There is significant spatial variation in the VPD trends, but overall, increases in VPD were observed for the majority of the study area (Figure 1). When averaged across the study period and the United States, significant increases in VPD have risen at a rate of approximately 0.007 kPa/yr, which extrapolates to a total of 0.25 kPa for the 35 year historical time period. VPD increased over the largest areal extent of land during the summer season, for which, 25% of the total number of grid points showed a statistically significant increase and 0.74% showed a significant decrease. The positive trends were largely concentrated in the western and southern portion of the United States and the upper Midwest, while the only significant decreases in VPD were found in western Montana. Both the Spring and Fall seasons exhibited a similar amount of significant increases in VPD (spring = 17.2% statistically significant increases; fall = 18.6%) and a minor amount of VPD decreases (spring = 2.4% statistically significant decreases; fall = 0.5%). These increases were largely concentrated in the southwestern United States. The fall season, however, was associated with a large area of statistically significant increases in the upper Midwest. It is worth noting the large area of decreasing VPD in the upper Great Plains stretching from eastern Montana to Minnesota during the spring season. Lastly, the winter season did not exhibit a large number of grid points with statistically significant increases (2.2%) or decreases (2.0%).

The changes in VPD for the historical time period were a result in directional or divergent changes in e_s and e_a (Figure 1). The e_s increased for a large portion of the United States for the spring, summer, and fall seasons. No large areas of significant e_s trends occurred for the winter season except for a portion of the southern United States. Figure 1 indicates that trends in e_s were largely correlated to trends in VPD (winter correlation: 0.66, spring correlation: 0.81, summer correlation: 0.81, fall correlation: 0.57), though important distinctions do arise. For example, significant increases in winter e_s occurred for the southern United States (Texas and Louisiana), but this area did not show significant changes in winter VPD.

The e_a decreased for a large portion of the United States for all seasons (Figure 1). Significant decreasing e_a trends were largely concentrated in the southwestern United States, while the northeastern United States showed areas of increasing e_a for the winter, summer, and fall time periods. These patterns correspond to precipitation trends found in other work [Prein et al. [2016]; Ficklin et al., 2016b]. The e_a decreasing trends negatively corresponded to increases in VPD (winter correlation: -0.27 , spring correlation: -0.61 , summer correlation: -0.75 , fall correlation: -0.72).

Figure 1 indicates that e_s and e_a did not increase or decrease in tandem or at the same magnitude, resulting in changes to VPD. The e_s generally increased faster than e_a (Figure S1 in the supporting information). This is especially true for the summer and fall seasons, where e_a increased faster than e_s for only a small area of the United States (11% for the summer and 8.0% for the fall). The winter and spring seasons showed larger areas where e_a increased faster than e_s (38.9% for the winter and 32.1% for the spring), but overall the e_s trend still dominated the e_a trend.

The differences in e_s and e_a (and therefore VPD) stemmed from recent changes in air temperature (Figure 2). Significant increases in maximum and minimum air temperature increased in tandem for all seasons and was especially apparent for the summer and fall, where nearly all of the United States exhibited increases in both maximum and minimum air temperature. The average maximum air temperature increase for the United States was 0.014 (winter), 0.013 (spring), 0.024 (summer), and 0.026 (fall) °C/yr. The average minimum air temperature increase for the United States was 0.017 (winter), 0.013 (spring), 0.027 (summer), and 0.023 (fall) °C/yr. These trends are slightly smaller than the 1979–2004 trends estimated by Vose et al. [2005]. The Vose

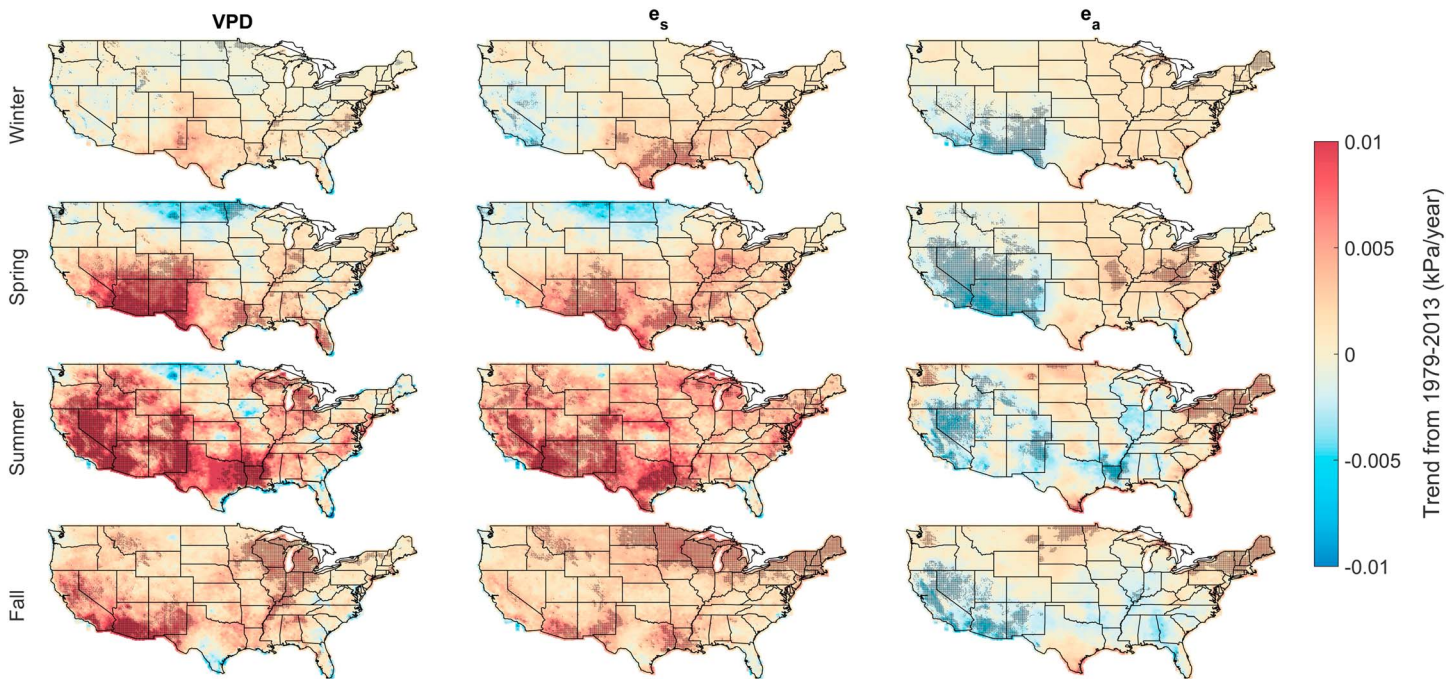


Figure 1. Trends of vapor pressure deficit (VPD), saturation vapor pressure (e_s) and actual vapor pressure (e_a) from 1979 to 2013 for all seasons. The hatched regions represent a significant trend at $p < 0.05$.

et al. [2005] study also indicated no significant change in diurnal temperature range. The result that minimum temperature increased at approximately the same rate contradicts previous work suggesting that historic minimum temperature increased faster than the daily average temperature [Roderick and Farquhar, 2002], though that result is dependent on the time period used [Vose *et al.*, 2005; Ficklin *et al.*, 2016b]. In the Roderick and Farquhar [2002] study, though, the minimum temperature is surrogated to the dew point temperature, and the rapid increase in minimum temperature reported is interpreted in Roderick and Farquhar [2002] as evidence that changes in historic VPD are negligible.

Relative humidity was negatively related to air temperature and significantly decreased for large portion of the United States for all seasons, especially the summer and fall (Figure 2). The largest spatial extent of relative humidity decreases were found for the summer and fall seasons, with an average decrease of -0.07 and $-0.09\%/yr$, respectively. The largest relative humidity decreases were found in the southwestern United States.

3.2. Projected Changes in Vapor Pressure Deficit, Saturation Vapor Pressure, and Actual Vapor Pressure

GCM projections were assessed in order to determine if the historical trends are projected to continue into the future. To assess the historical accuracy of the downscaled GCMs, we spatially and temporally compared observed Summer VPD from the METDATA observations to historical summer VPD from the MACA GCM data set. Minimal spatial and magnitude differences were found for the observed and historical GCM data (Figure 3). Compared to the observed, METDATA VPD, the downscaled GCMs accurately estimate areas of high VPD in the southwestern United States and areas of low VPD in the Pacific Northwest and eastern United States.

To compare temporal trends in the model and observed data, we aggregated the $>20,000$ grid points into National Centers for Environmental Information climate regions based on the work of Karl and Koss [1984] resulting in nine climate regions (Figure S2). Within each region, the average of VPD, e_s , and e_a for all grid points for all climate data sets (METDATA, GCM ensemble) were averaged. This results in one time series for each region for each climate data set. Figure 4 displays monthly METDATA, GCM ensemble median, GCM ensemble range averaged for each climate region from 1979 to 2013. As was the case for the spatial

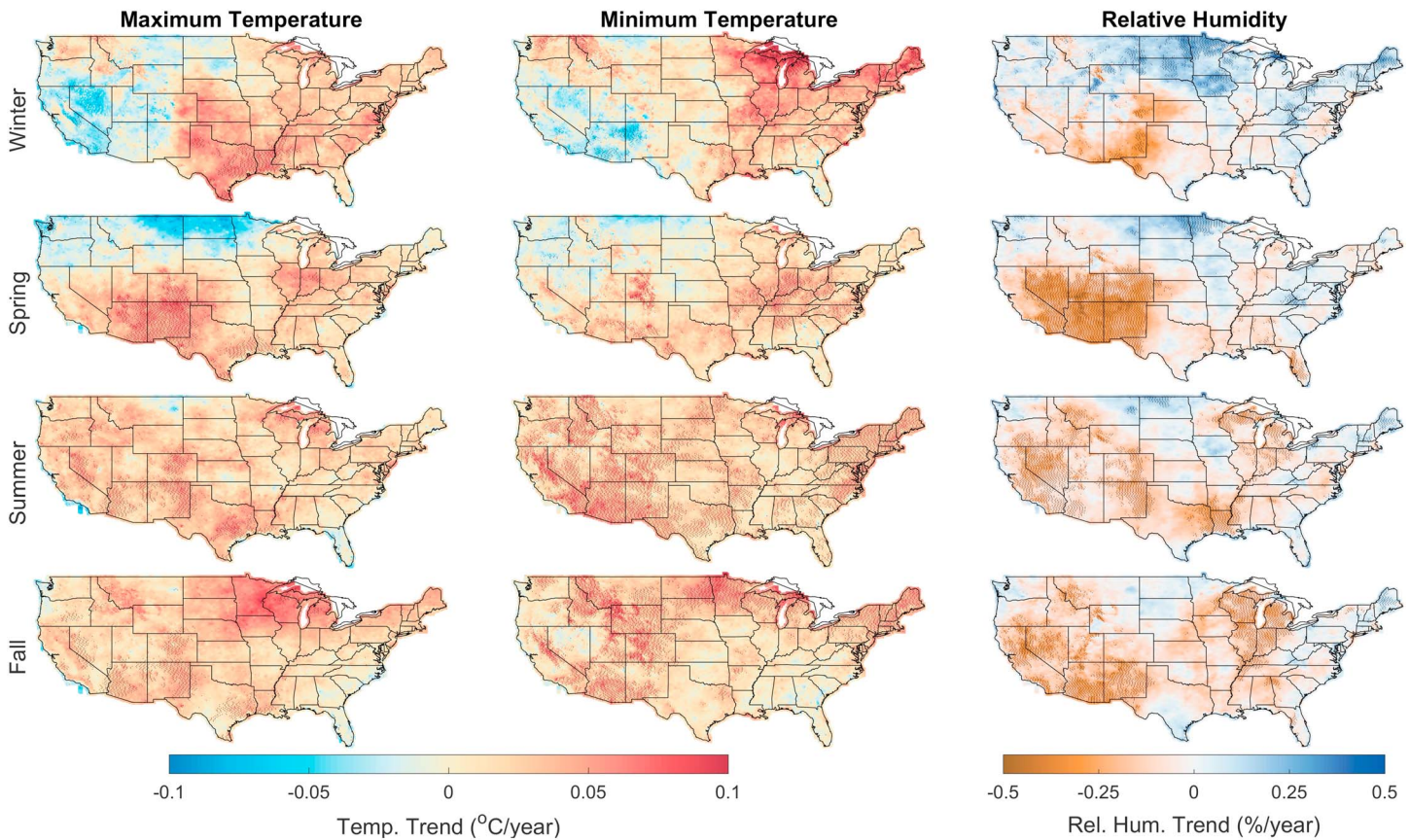


Figure 2. Trends of maximum air temperature, minimum air temperature, and relative humidity from 1979 to 2013 for all seasons. The hatched regions represent a significant trend at $p < 0.05$.

comparisons of the observed and historical GCM time periods, the downscaled GCMs adequately capture the magnitude and timing of VPD for each region, even though there is variation around the GCM ensemble median. Figures S3 and S4 display the same temporal information, but for e_s and e_a .

Nearly every model projects a large increase in VPD in the future relative to the historic time period. Figure 5 presents percent differences between historical and projected time periods in summer VPD for the 18 GCM ensemble first quartile, median, and third quartile for the 2065–2099 time period. Projections for each GCM are shown in Figures S5–S7 for VPD, e_s , and e_a . To get a sense on how much the GCM projections temporally vary, we also show the temporal results of the projections of the GCM ensemble median and GCM ensemble range for all months using similar methods as previously discussed (Figure 6 for VPD; Figure S8 for e_s ; Figure S9 for e_a); however, because we are comparing observed and projected VPD, e_s , and e_a , we show projected percent changes compared to the historical time period (i.e., January 2080 compared to average of all historical January VPD). Results are for the highest emission pathway (RCP 8.5). Therefore the results presented can be thought of as a constraint on the “maximum” change in VPD and its components, but noting that previous work [Sanford *et al.*, 2014] indicates that we are currently following the RCP 8.5 pathway.

The GCMs project large increases in VPD during Summer (Figure 5). The GCM ensemble VPD median for the United States is a 0.72 kPa (51% percent change) increase compared to the historical time period, with an increase of 0.55 (39%) and 0.88 kPa (64%) for the first and third quartile for the GCM ensemble, respectively. This 0.72 kPa median increase is consistent with the trend of significant trends observed during the 35 year historical time period when extrapolated to the projected time period. The smallest projected VPD increase is 0.32 kPa (GCM MRI-CGCM3) and the largest increase is 1.12 kPa (HadGEM2-ES365) (Figure S5). Temporally, the percent change variation around the projected GCM ensemble median is large for VPD, with the Upper Midwest and Northern Rockies and Plains having the largest GCM uncertainty (~15% to >200% change

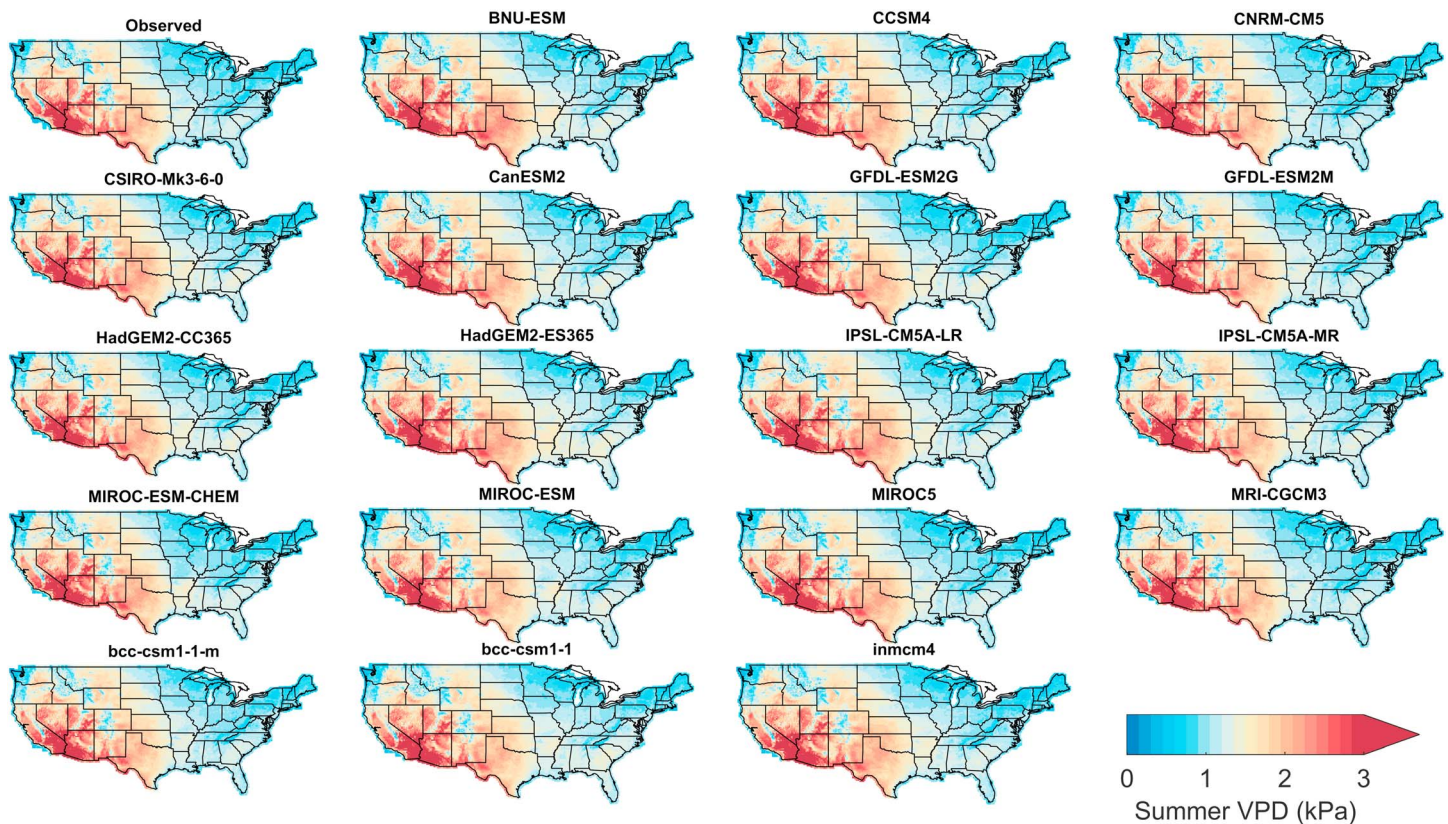


Figure 3. Spatial comparison between average summer vapor pressure deficit (VPD) for the observations from the METDATA data set and the GCM historical time period (1979–2013) from the MACA data set.

from historical to projected VPD; Figure 6). Importantly, however, nearly all models predict an increase in VPD for each region.

Nearly all GCMs (18) are in agreement that VPD will increase for the United States relative to the historical time period (Figures 6 and 7). A smaller number of GCMs agree that VPD will increase by at least 0.5 kPa when compared to the number that agrees that VPD will increase by some amount >0 kPa, but there is still a concurrence among the vast majority of the GCMs (~ 15 GCMs) that VPD for much of the United States will increase by 0.5 kPa. The coastal areas, northeastern United States, and the high-elevation regions in the western United States do not show a concurrence of a VPD increase >0.5 kPa (1–5 GCMs). Lastly, much of the United States does not show a clear agreement on a 1 kPa increase. The only areas that do are the extremely arid regions of Arizona, California, and Nevada (14–16 GCMs) and southern central Great Plains (8–11 GCMs).

Due to its sole dependence on air temperature (equations 1–3), summer e_s is projected to considerably increase (Figure 5 and Figures S6 and S8) with a GCM ensemble median increase of 1.07 kPa (35% percent change) and a first and third quartile increase of 0.87 (29%) and 1.27 kPa (42%) compared to the historical time period. The temporal uncertainty is similar to the VPD temporal uncertainty, with both the Upper Midwest and Northern Rockies and Plains having large uncertainties (Figure S8). Overall, the GCM uncertainties are less when compared to the VPD GCM uncertainties, and again, most models predict an increase in e_s of between future and present conditions.

There is clear agreement among GCMs that e_s will increase by at least 0.5 kPa relative to the historical time period (Figure 7). This agreement decreases when the threshold is changed to at least a 1 kPa increase, but there is still a large concurrence. Large portions of the eastern and western United States do not meet this threshold (1–5 GCMs in agreement), while there is some agreement in the central United States (10–12 GCMs) and clear agreement in the extremely arid regions of the western United States and the south central Great Plains (12–18 GCMs).

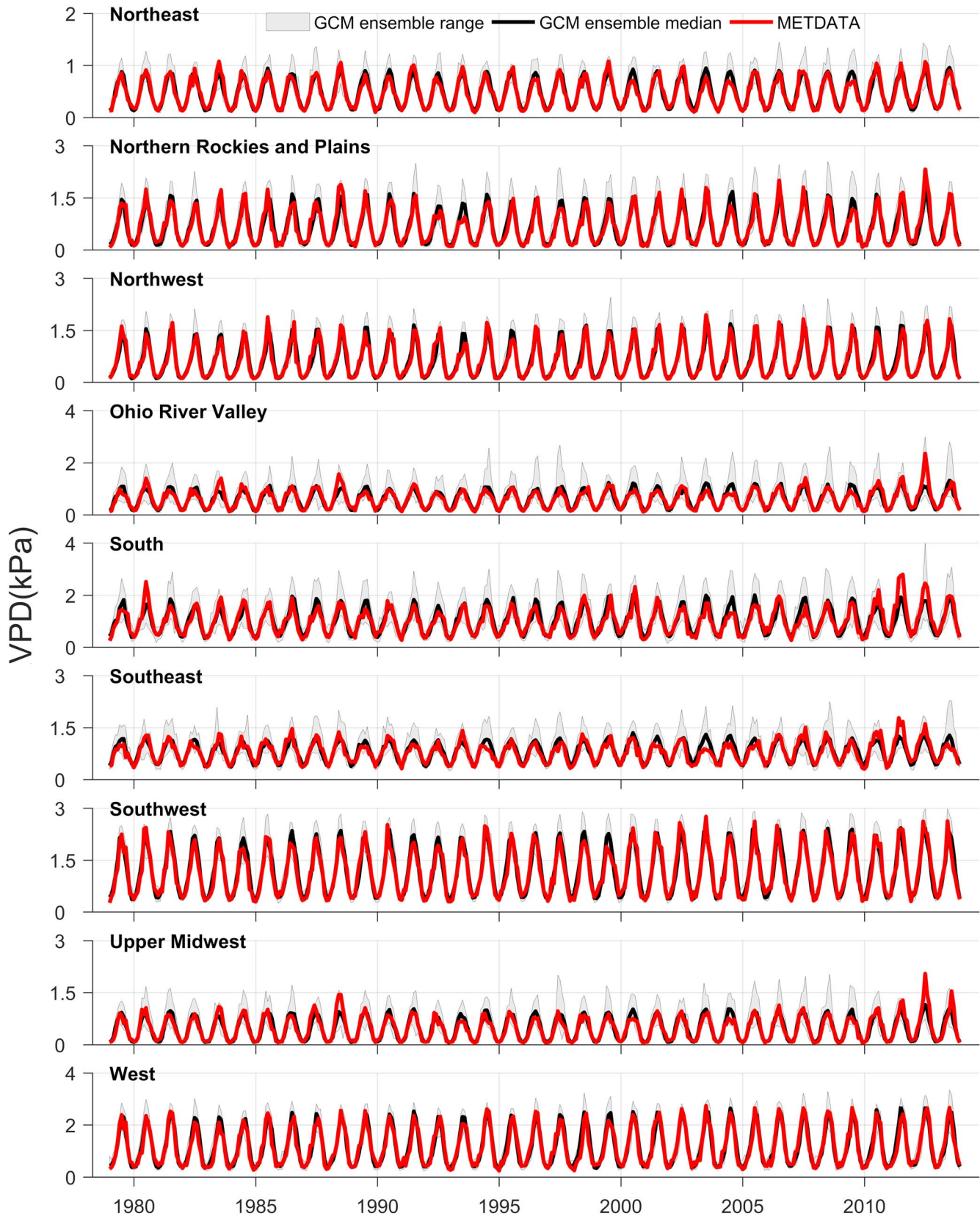


Figure 4. Temporal comparison between vapor pressure deficit (VPD) for the observations from the METDATA data set and the GCM historical time period (1979–2013) from the MACA data set for each climate region defined by *Karl and Koss* [1984] and shown in Figure S2 of the supporting information.

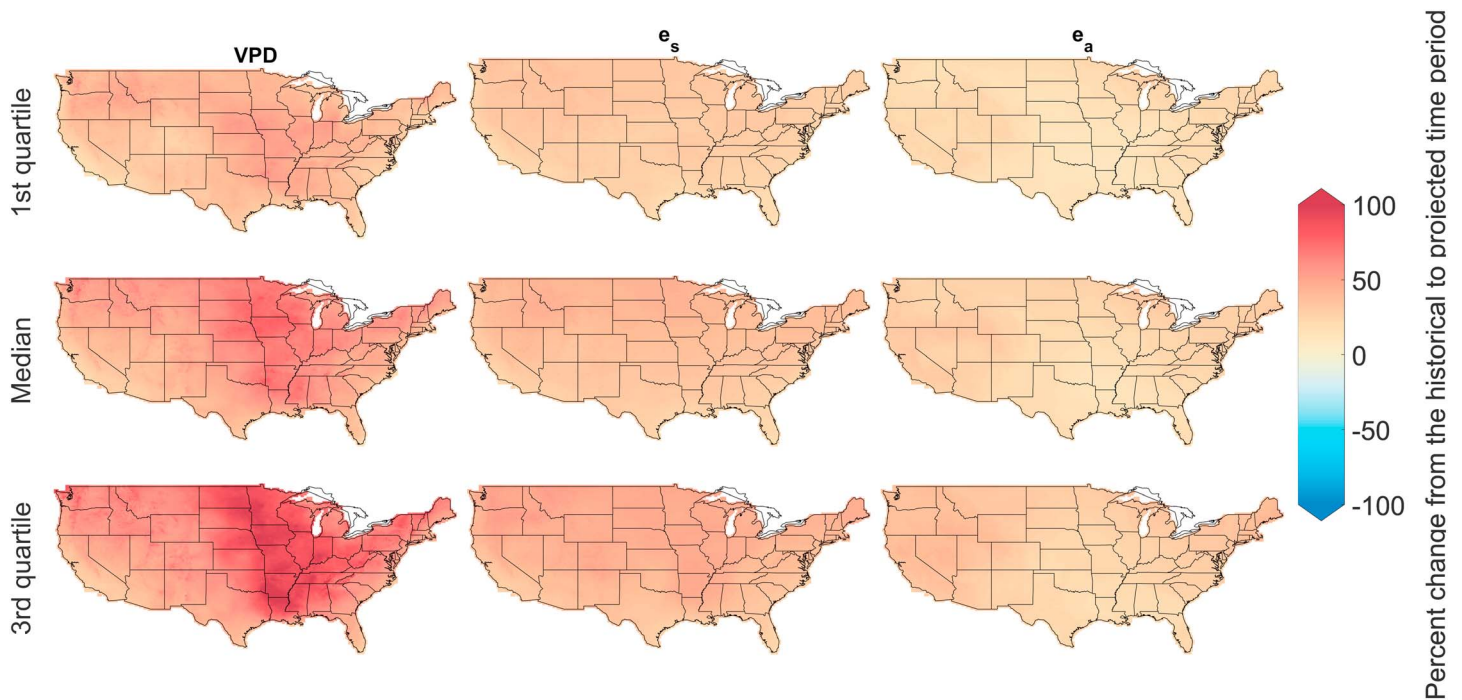


Figure 5. GCM ensemble median and quartiles of changes between the historical (1979–2013) and projected (2065–2099) time periods for summer vapor pressure deficit (VPD), saturation vapor pressure (e_s), and actual vapor pressure (e_a).

While summer e_s is projected to increase considerably, summer e_a is not projected to change as much, resulting in the large projected increases in VPD (Figures 5 and 7). The GCM ensemble median indicates a 0.35 kPa (23% percent change) increase compared to the historical time period, approximately one third less than the projected change in e_s . The first and third quartiles also show consistent e_a increases, with 0.27 (18%) and 0.43 kPa (28%) increases, respectively. The temporal GCM uncertainties display similar uncertainties as the e_s GCM uncertainties, though the overall e_a increase is less (Figure S9).

While both e_s and e_a are projected to increase, the rate of increase of e_s eclipses the rate of increase of e_a , and only a few GCMs—and for small areal extents—project that e_a will increase faster than e_s (Figure S10). Compared to VPD and e_s , there is not a clear agreement among GCMs of large increases in e_a (Figure 7). While all GCMs agree that e_a will increase, no clear agreement can be found for the 0.5 or 1 kPa threshold. The only area where there is some agreement on a 0.5 kPa threshold is the central portion of the eastern United States (Virginia, North Carolina, and South Carolina).

The projected summer increases in maximum and minimum temperatures are the reason for increases in e_s (Figures S11 and S12). The GCM ensemble median increase in maximum temperature is 5.3°C (first quartile: 4.4°C; third quartile: 6.0°C), and no GCM projects an increase less than 3.0°C. The same is true for minimum temperature where the GCM ensemble median increase is 4.8°C (first quartile: 3.9°C; third quartile: 6.0°C) with the smallest increase of 3.4°C (GCM inmcm4) (Figures S11 and S12).

The small increases in e_a relative to e_s are linked to decreases or minimal changes in summer relative humidity (Figures 8 and S13). The GCM ensemble median for the United States indicates a projected decrease in relative humidity of approximately 4.4% with a first and third quartile decrease of 6.4 and 2.8%, respectively (Figure 8). The decrease in relative humidity is a robust result among GCMs (Figure 9), with near concurrence for most of the United States. While there is agreement of a projected relative humidity decrease, the decreases are small (5%) compared to the historical time period for a large portion of the United States. In the central United States, however, an agreement among GCMs of a relative humidity decrease is greater than 5%, but not necessarily 10% (Figure 9).

These declines in relative humidity, which contradict assumptions of constant global (land and ocean) relative humidity that inform many climate studies [Dessler and Sherwood, 2009; Held and Soden, 2006]

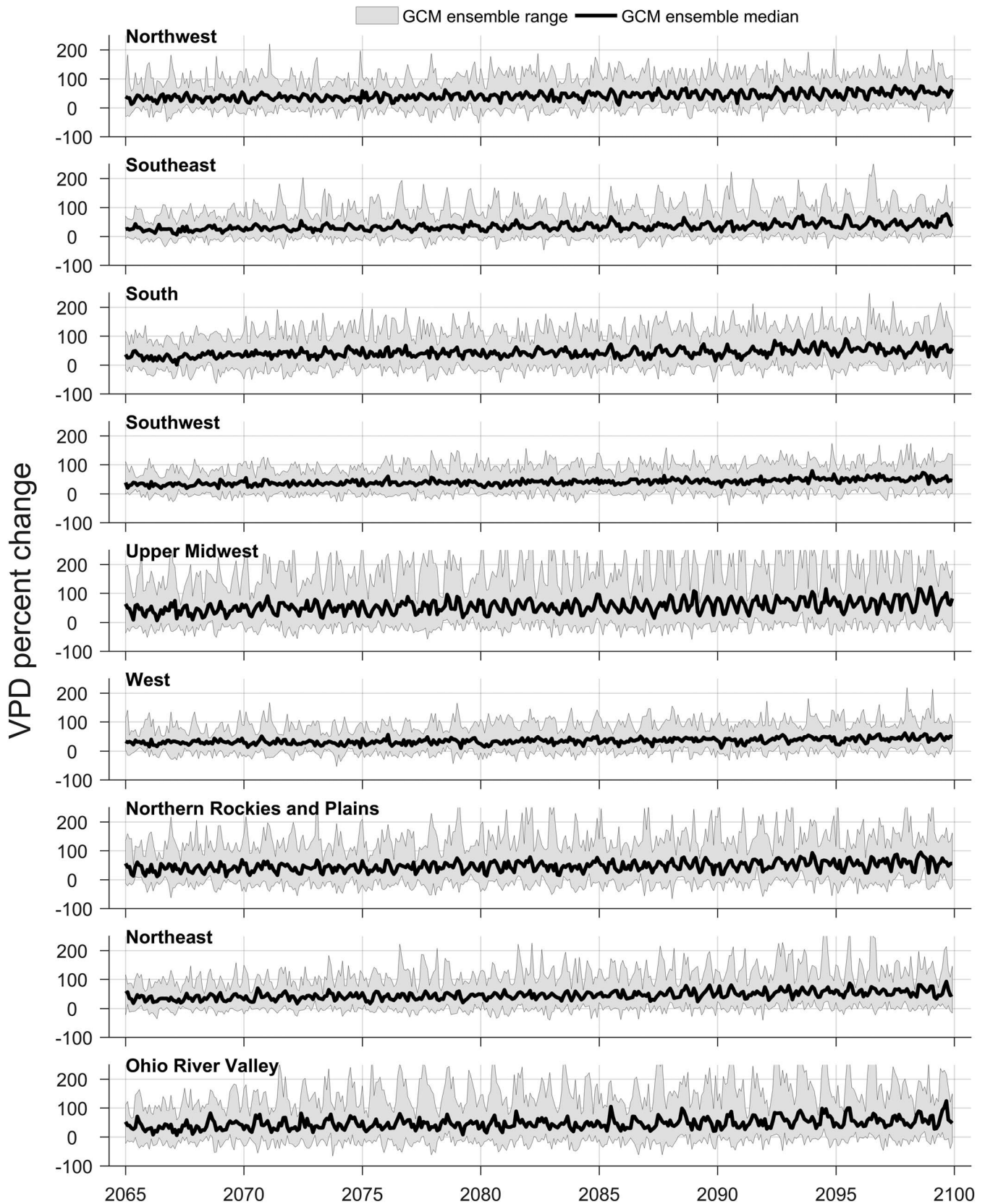


Figure 6. Temporal agreement/uncertainty for monthly percent change in projected (2065–2099) vapor pressure deficit (VPD) compared to the historical (1979–2013) time period for the GCM ensemble for each climate region defined by Karl and Koss [1984] and shown in Figure S2.

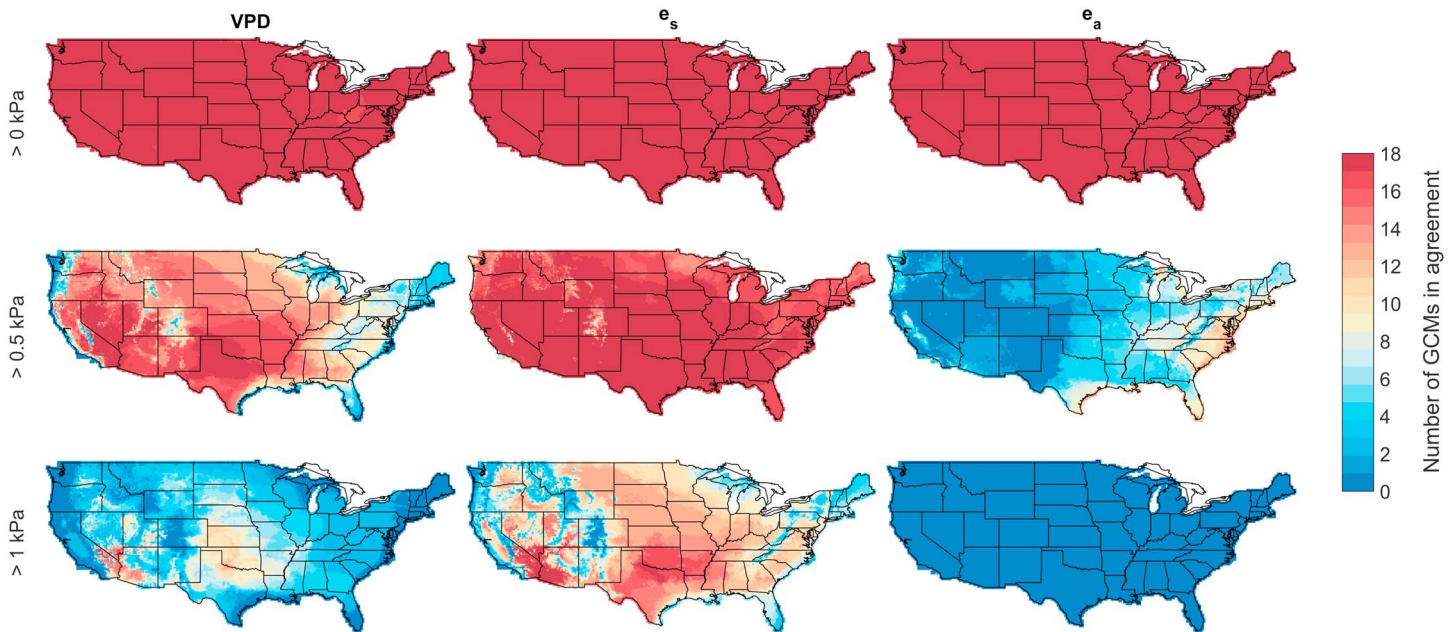


Figure 7. Agreement among GCMs on increases by at least 0 kPa, 0.5 kPa, or 1.5 kPa for summer vapor pressure deficit (VPD), saturation vapor pressure (e_s), and actual vapor pressure (e_a) compared to the historical time period (1979–2013).

have several potential causes, all of which ultimately reflect limitations to terrestrial evapotranspiration. Simply put, rising temperatures create more “room” in the atmosphere for water vapor by increasing the saturation vapor pressure, but over terrestrial surfaces, the movement of water from land to the atmosphere is impeded one way or another, preventing the actual vapor pressure from keeping pace with temperature-driven increases in e_s [Byrne and O’Gorman, 2016]. The same argument does not necessarily apply over oceans, where temperature is rising more modestly and moisture supply to the atmosphere is not limited. As a result, ocean relative humidity is projected to be more stable in time [Byrne and O’Gorman, 2016].

It is also important to note that an increase in VPD would be expected under warmer temperatures even if relative humidity were constant, driven by the exponential relationship between e_s and temperature (i.e., equations (1) and (2)). However, our results demonstrate that estimated historic and projected future changes in VPD are strongly linked to the fact that, over land, e_a has historically not risen as quickly as e_s (and in some places has decreased), a trend which we project will continue into the future. Some previous studies have proposed that this decoupling between terrestrial e_a and e_s is principally driven by coarse-scale air circulation patterns, where air transported to land from the relatively cooler and more slowly warming oceans keeps the e_a over land from rising as quickly as e_s [Sherwood and Fu, 2014; Fu and Feng, 2014; Fasullo, 2010]. However, other recent work highlights the importance of limitations to terrestrial evapotranspiration as another important constraint on the rate of increase of terrestrial e_a [Byrne and O’Gorman, 2016; Berg et al., 2016], with some studies reporting recent declines in evapotranspiration that cannot be explained by changes in radiation [i.e., global dimming; Jung et al., 2010; Ridgen and Salvucchi, 2016].

3.3. Projected Changes in Stomatal Conductance

Other factors that are proposed to be significantly limiting to evapotranspiration include reductions in soil moisture supply [Jung et al., 2010; de Jeu et al., 2008] or stomatal closure under elevated CO_2 [Ainsworth and Rogers, 2007; Medlyn et al., 2001]. The results from this study suggest that increasing VPD itself may drive forward a feedback cycle whereby plants close their stomates to prevent excessive water loss, promoting significant declines in stomatal conductance that will be limiting to evapotranspiration and thereby further reduce the rate of increase of e_a . This line of inference is supported by other recent work relying on observations of ecosystem water cycling to demonstrate VPD-driven limitations to stomatal functioning

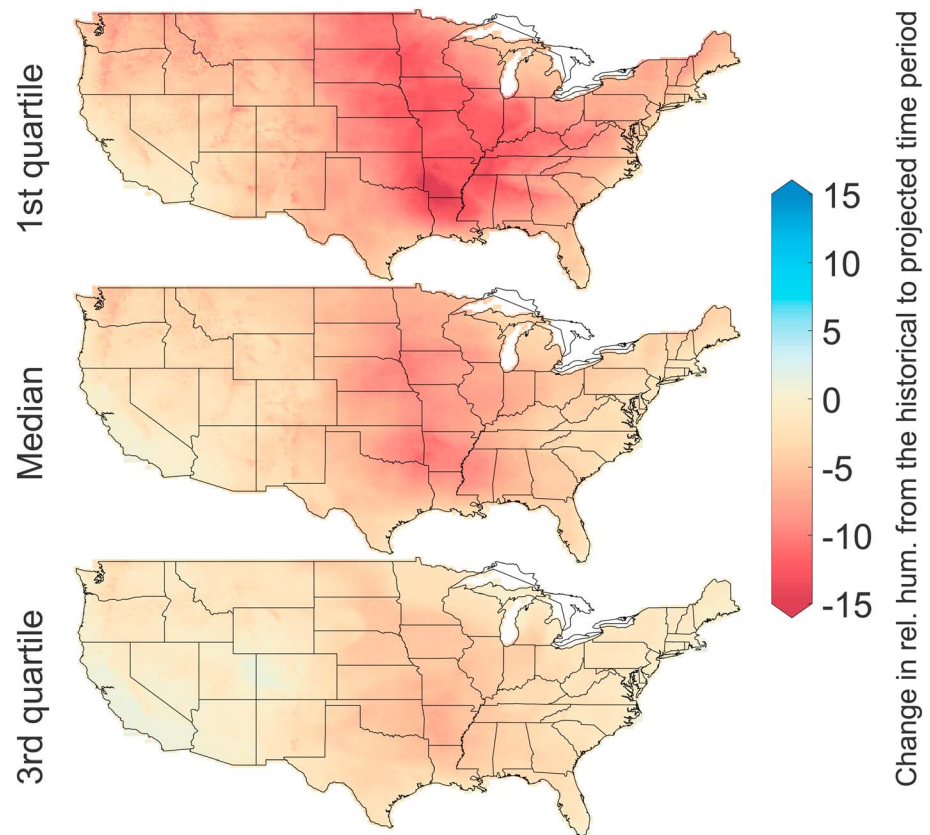


Figure 8. GCM ensemble median and quartiles of changes between the historical (1979–2013) and projected (2065–2099) time periods for summer relative humidity.

[Bonan *et al.*, 2014; Sato *et al.*, 2015; Novick *et al.*, 2016; Sperry *et al.*, 2016], and an observed recent decline in evapotranspiration over the continental United States that can only be explained if VPD-driven reductions to stomatal conductance are considered [Rigden and Salvucci, 2016].

Due to the inverse relationship between g_s and VPD predicted by Darcy's law (i.e., equations (8) and (9)), the relative change in g_s driven by historic changes in VPD is not necessarily correlated with the magnitude of VPD change. For example, in areas of the central and eastern United States where VPD change is small, we nonetheless found significant, historic changes in summer g_s due to the high sensitivity of g_s to VPD when VPD is low (Figure S14). However, the analysis nonetheless also suggests a significant decline in historic g_s for much of the western United States where VPD has historically increased. Moving forward, however, the analysis suggests that all regions of the United States are projected to experience VPD-driven declines in g_s on the order 30% for the entire continental United States, and 35% for the relatively mesic eastern U.S. under the assumption of stationarity (Figure 10 for the GCM median and quartiles—left column and Figure S15 for all GCMs).

We again reiterate that these historic and future projections for g_s shown in Figure 10 rely on the simplifying assumption that $T_r = K(\Psi_S - \Psi_L - \rho gh)$ is constant with time. In reality, long-term, adaptive variation in K may be realized as changes in leaf area, sapwood-to-leaf area ratio, or canopy height [McDowell *et al.*, 2002; Novick *et al.*, 2009; Piao *et al.*, 2006]. The soil-to-leaf water potential difference may be independently affected by variation in soil moisture content (affecting Ψ_S), canopy height (affecting ρgh), and shifts in whether plants regulate Ψ_L to be relatively constant (isohydric) or adaptive (anisohydric) [McDowell and Allen, 2015; Roman *et al.*, 2015; Martínez-Vilalta *et al.*, 2014]. Changes in these other factors do not uniformly decrease or increase g_s . For example, increases in K driven by adaptive adjustments to hydraulic architecture will tend to increase g_s , whereas decreases in future soil moisture will tend to decrease g_s .

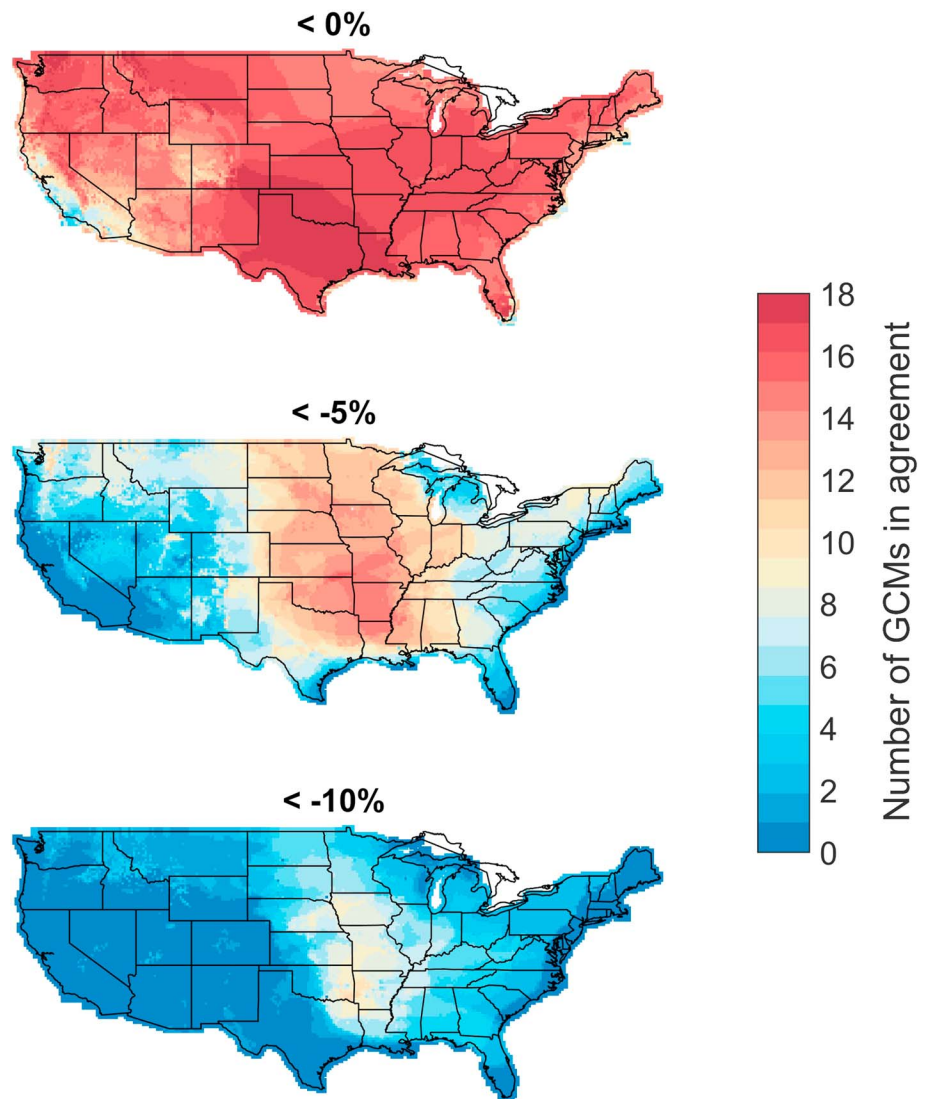


Figure 9. Agreement among GCMs on projected (2065–2099) decreases by at least 0%, 5%, or 10% for summer relative humidity compared to the historical (1979–2013) time period.

To this end, we also include changes in g_s from (1) a 30% decline in soil water potential (Figure 10, middle column for GCM ensemble median and quartiles and Figure S16 for all GCMs) estimated from equation (9) and (2) a 30% adaptive increase in K (Figure 10, right column for GCM ensemble median and quartiles and Figure S17 for all GCMs) as estimated by equation (12) as a way to bracket the uncertainty. When a 30% decline in soil water potential is assumed, the GCM median ensemble decrease in g_s changes from 30% under the stationarity assumption to a 51% decrease. When a 30% adaptive increase in K is included, the g_s becomes more modest (a 9% decrease on average), where approximately 6% of the grid cells showed an increase in g_s under future climates.

These reductions in g_s have important implications for land-atmosphere interactions. On the one hand, reductions in g_s due to rising VPD could limit evapotranspiration [Rigden and Salvuchhi, 2016] in a matter similar to reductions in g_s driven by rising CO_2 , representing a feedback that could further accelerate the rate of increase in atmosphere demand. However, with regard to that feedback, it is important to note that our estimates likely overstate the importance of decreases in g_s with projected VPD in determining regional patterns of evapotranspiration and atmospheric demand for two reasons: (1) the entire United States is not completely covered in vegetation (i.e., urban areas, desert regions) and (2) each pixel where g_s is

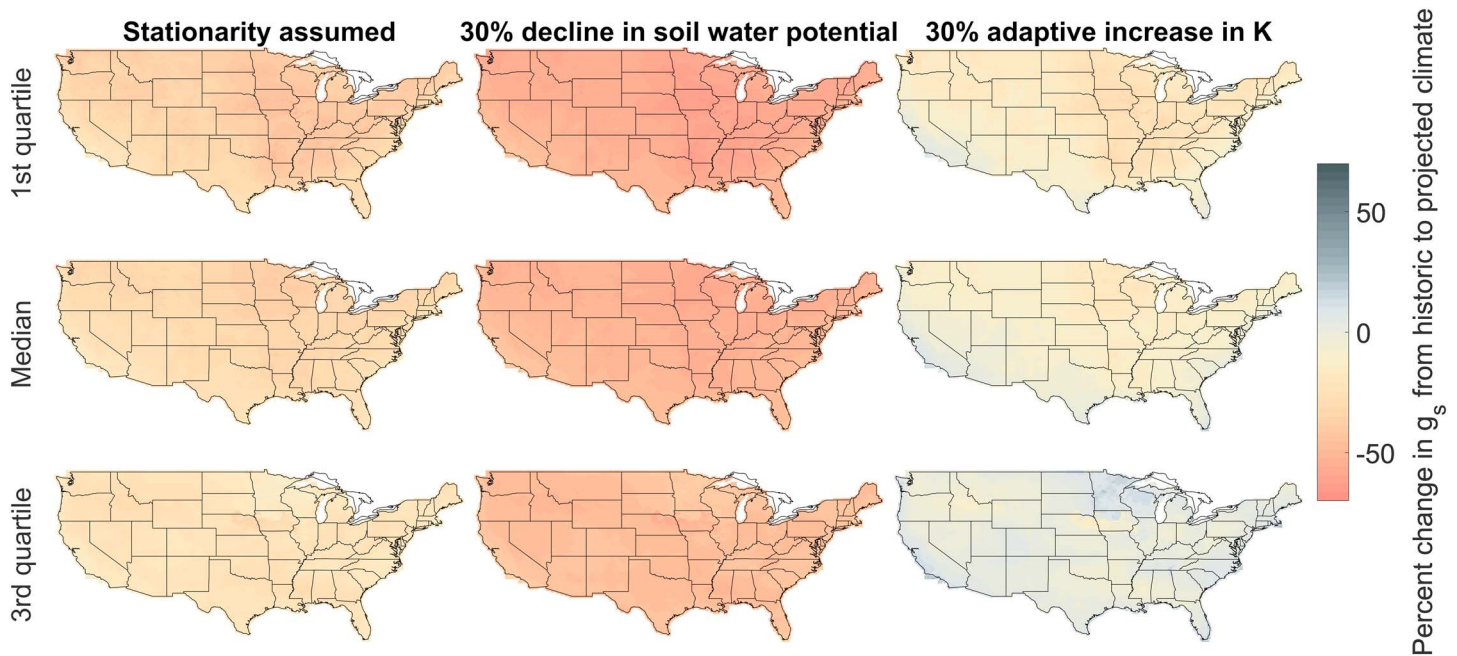


Figure 10. GCM ensemble median and quartiles of percent changes between the historical (1979–2013) and projected (2065–2099) time periods for summer stomatal conductance (g_s) assuming (left column) stationarity, (middle column) a 30% decline in soil water potential, and (right column) a 30% adaptive increase in K .

estimated may not be completely covered with vegetation (i.e., a mix of urban and forest). Therefore, the decreases in g_s presented here should be viewed as a lower bound when considering VPD effects on g_s at the scale of a grid cell. On the other hand, reductions in g_s from rising VPD will reduce the rate of vegetative carbon uptake, noting that changes in plant intrinsic water use efficiency may prevent reductions to photosynthesis from being as severe as reduction to g_s [Medlyn *et al.*, 2011, Katul *et al.*, 2009]. In this case, the projected decline in leaf level g_s and carbon assimilation due to rising VPD, which is important for determining individual-scale growth and fitness, does not necessarily depend on the fraction of vegetation cover in each grid cell. However, the consequences of VPD-driven stomatal closure for regional and global carbon cycling will be more strongly determined by densely vegetated areas that tend to be high carbon sinks.

The magnitude and range of these estimated responses are on the same order as the estimated declines in g_s linked to increasing water use efficiency with rising CO_2 (~20%) [Ainsworth and Rogers, 2007; Katul *et al.*, 2009; Medlyn *et al.*, 2011]. Both CO_2 - and VPD-driven declines in stomatal conductance will affect transpiration and thereby affect hydrologic cycling [Milly and Dunne, 2016]. Rising CO_2 is generally recognized to enhance carbon uptake in spite of associated reductions in g_s [Ainsworth and Rogers, 2007]. In contrast, while water use efficiency may also increase with rising VPD [Novick *et al.*, 2009], much empirical evidence exists to suggest that gross and net primary productivity are limited under high VPD [Eamus *et al.*, 2013; Lasslop *et al.*, 2010]. As a result, VPD-driven reductions in future g_s may offset gains in photosynthesis associated with rising CO_2 .

4. Summary and Conclusions

VPD represents the ability of the air to extract moisture from the land surface, defined as the difference between the water vapor in the air at saturation (e_s) and the actual amount of water vapor (e_a). We examine changes in VPD, e_s , e_a , and their underlying climatic components in the United States for the observed, recent past (1979–2013) and the future (2065–2099) using an ensemble of 18 GCMs from the high-emission pathway RCP 8.5. We find significant increases in VPD for nearly all seasons in the recent past from diverging trends in e_s owing to increases in air temperature and decreases in e_a from decreases in relative humidity. These trends are especially apparent in the southwestern United States, which has shown to be especially

sensitive to forest mortality from increases in temperature [McDowell and Allen, 2015; Williams et al., 2014, 2013].

The GCM ensemble also indicates that VPD will continue to increase into the future from larger increasing trends in e_s as compared to e_a . The e_s is projected to significantly increase for the United States, while e_a increases are minor. The large e_s increases are related to increases in air temperature. The minor e_a increases, on the other hand, imply limitations to the rate at which water vapor is supplied to the atmosphere, which have the effect of reducing relative humidity and increasing VPD. Using a simple model for plant hydraulic functioning, we estimated that future changes in VPD can reduce stomatal conductance by ~9–51%, which is a magnitude comparable to the expected decline in g_s from rising CO₂.

Acknowledgments

All data used in this work are available at <http://metdata.northwestknowledge.net/> for the historical climate data and maca.northwestknowledge.net for the projected climate data. These data sets are included in the references. We thank Ben Sulman, Alex Konings, Tae Hee Hwang, Eric Ward, and Sally Letsinger for helpful feedback. We acknowledge the World Climate Research Programme's Working Group on Coupled Modeling for the CMIP, and we thank the climate modeling groups for producing and making available their model output. For CMIP, the U.S. Department of Energy's Program for Climate Model Diagnosis and Intercomparison provides coordinating support and led development of software infrastructure in partnership with the Global Organization for Earth System Science Portals. K. Novick acknowledges funding from National Science Foundation grant DEB-1552747 and the Ameriflux Management Project sponsored by the U.S. Department of Energy through Lawrence Berkeley National Lab.

References

- Abatzoglou, J. T. (2013), Development of gridded surface meteorological data for ecological applications and modelling, *Int. J. Climatol.*, *33*(1), 121–131.
- Abatzoglou, J. T., and T. J. Brown (2012), A comparison of statistical downscaling methods suited for wildfire applications, *Int. J. Climatol.*, *32*(5), 772–780.
- Ainsworth, E. A., and A. Rogers (2007), The response of photosynthesis and stomatal conductance to rising CO₂: Mechanisms and environmental interactions, *Plant Cell Environ.*, *30*(3), 258–270.
- Allen, R. G., L. S. Pereira, D. Raes, and M. Smith (1998), Crop evapotranspiration—Guidelines for computing crop water requirements—FAO Irrigation and drainage paper 56, *FAO, Rome*, 300, 6541.
- Berg, A., et al. (2016), Land-atmosphere feedbacks amplify aridity increase over land under global warming, *Nat. Clim. Change*, doi:10.1038/NCLIMATE3029.
- Bohren, C. F., B. A. Albrecht, and D. V. Schroeder (2000), Atmospheric thermodynamics, *Am. J. Phys.*, *68*(12), 1159–1160.
- Bonan, G., M. Williams, R. Fisher, and K. Oleson (2014), Modeling stomatal conductance in the Earth system: linking leaf water-use efficiency and water transport along the soil–plant–atmosphere continuum, *Geosci. Model Dev.*, *7*, 2193–2222.
- Breshears, D. D., H. D. Adams, D. Eamus, N. G. McDowell, D. J. Law, R. E. Will, A. P. Williams, and C. B. Zou (2013), The critical amplifying role of increasing atmospheric moisture demand on tree mortality and associated regional die-off, *Front. Plant Sci.*, *4*, 266.
- Byrne, M. P., and P. A. O'Gorman (2016), Understanding decreases in land relative humidity with global warming: Conceptual model and GCM simulations, *J. Am. Met. Soc.*, doi:10.1175/JCLI-D-16-0351.1.
- Clapp, R. B., and G. M. Hornberger (1978), Empirical equations for some soil hydraulic properties, *Water Resour. Res.*, *14*, 601–604, doi:10.1029/WR014i004p0601.
- Cowan, I. R., and G. D. Farquhar (1977), Stomatal function in relation to leaf metabolism and environment, *Symp. Soc. Exp. Biol.*, *31*, 471–505.
- Daly, C., M. Halbleib, J. I. Smith, W. P. Gibson, M. K. Doggett, G. H. Taylor, J. Curtis, and P. P. Pasteris (2008), Physiographically sensitive mapping of climatological temperature and precipitation across the conterminous United States, *Int. J. Climatol.*, *28*(15), 2031–2064.
- de Jeu, R. A. M., W. Wagner, T. R. H. Holmes, A. J. Dolman, N. C. van de Giesen, and J. Friesen (2008), Global Soil Moisture Patterns Observed by Space Borne Microwave Radiometers and Scatterometers, *Surv. Geophys.*, *29*(4), 399–420.
- Dessler, A. E., and S. C. Sherwood (2009), A matter of humidity, *Science*, *323*(5917), 1020–1021.
- Eamus, D., N. Boulain, J. Cleverly, and D. D. Breshears (2013), Global change-type drought-induced tree mortality: Vapor pressure deficit is more important than temperature per se in causing decline in tree health, *Ecol. Evol.*, *3*(8), 2711–2729.
- Fasullo, J. T. (2010), Robust land-ocean contrasts in energy and water cycle feedbacks, *J. Clim.*, *23*(17), 4677–4693.
- Ficklin, D. L., J. T. Abatzoglou, S. M. Robeson, and A. Dufficy (2016a), The influence of climate model biases on projections of aridity and drought, *J. Clim.*, *29*, 1269–1285, doi:10.1175/JCLI-D-15-0439.1.
- Ficklin, D. L., S. M. Robeson, and J. H. Knouft (2016b), Impacts of recent climate change on trends in baseflow and stormflow in United States watersheds, *Geophys. Res. Lett.*, *43*, 5079–5088, doi:10.1002/2016GL069121.
- Fowler, H. J., S. Blenkinsop, and C. Tebaldi (2007), Linking climate change modelling to impacts studies: Recent advances in downscaling techniques for hydrological modelling, *Int. J. Climatol.*, *27*, 1547–1578, doi:10.1002/joc.1556.
- Fu, Q., and S. Feng (2014), Responses of terrestrial aridity to global warming, *J. Geophys. Res. Atmos.*, *119*, 7863–7875, doi:10.1002/2014JD021608.
- Hamlet, A. F., and D. P. Lettenmaier (2005), Production of temporally consistent gridded precipitation and temperature fields for the continental United States, *J. Hydrometeorol.*, *6*(3), 330–336.
- Hartmann, D. L., et al. (2013), Observations: atmosphere and surface, in *Climate Change 2013: The Physical Science Basis. Contribution of Working Group I to the Fifth Assessment Report of the Intergovernmental Panel on Climate Change*, edited by T. F. Stocker et al., pp. 159–254, Cambridge Univ. Press, Cambridge, U. K., and New York.
- Held, I. M., and B. J. Soden (2006), Robust responses of the hydrological cycle to global warming, *J. Clim.*, *19*(21), 5686–5699.
- Isaac, V., and W. A. van Wijngaarden (2012), Surface water vapor pressure and temperature trends in North America during 1948–2010, *J. Clim.*, *25*(10), 3599–3609.
- Johnson, F., and A. Sharma (2010), A comparison of Australian open water body evaporation trends for current and future climates estimated from Class A evaporation pans and general circulation models, *J. Hydrometeorol.*, *11*, 105–121.
- Jung, M., et al. (2010), Recent decline in the global land evapotranspiration trend due to limited moisture supply, *Nature*, *467*(7318), 951–954.
- Karl, T. R., and W. J. Koss (1984), Regional and national monthly, seasonal, and annual temperature weighted by area, 1895–1983, *Historical Climatology Series 4-3*, 38 pp., National Climatic Data Center, Asheville, N. C.
- Katul, G. G., S. Palmroth, and R. A. M. Oren (2009), Leaf stomatal responses to vapour pressure deficit under current and CO₂-enriched atmosphere explained by the economics of gas exchange, *Plant Cell Environ.*, *32*(8), 968–979.
- Kendall, M. G. (1975), *Rank Correlation Methods*, Griffin, London.
- Kunkel, K. E., T. R. Karl, D. R. Easterling, K. Redmond, J. Young, X. Yin, and P. Hennon (2013), Probable maximum precipitation and climate change, *Geophys. Res. Lett.*, *40*, 1402–1408, doi:10.1002/grl.50334.
- Lainé, A., H. Nakamura, K. Nishii, and T. Miyasaka (2014), A diagnostic study of future evaporation changes projected in CMIP5 climate models, *Clim. Dyn.*, *42*(9–10), 2745–2761.

- Lasslop, G., M. Reichstein, D. Papale, A. D. Richardson, A. Arneeth, A. Barr, P. Stoy, and G. Wohlfahrt (2010), Separation of net ecosystem exchange into assimilation and respiration using a light response curve approach: Critical issues and global evaluation, *Global Change Biol.*, *16*(1), 187–208.
- Leuning, R. (1995), A critical appraisal of a combined stomatal-photosynthesis model for C3 plants, *Plant Cell Environ.*, *18*(4), 339–355.
- Livneh, B., E. A. Rosenberg, C. Lin, B. Nijssen, V. Mishra, K. M. Andreadis, E. P. Maurer, and D. P. Lettenmaier (2013), A long-term hydrologically based dataset of land surface fluxes and states for the conterminous United States: Update and extensions, *J. Clim.*, *26*(23), 9384–9392.
- Lobell, D. B., G. L. Hammer, G. McLean, C. Messina, M. J. Roberts, and W. Schlenker (2013), The critical role of extreme heat for maize production in the United States, *Nat. Clim. Change*, *3*(5), 497–501.
- Mann, H. B. (1945), Nonparametric tests against trend, *Econometrica*, *13*(3), 245–259.
- Martínez-Vilalta, J., R. Poyatos, D. Aguadé, J. Retana, and M. Mencuccini (2014), A new look at water transport regulation in plants, *New Phytol.*, *204*(1), 105–115.
- Maurer, E. P., and D. W. Pierce (2014), Bias correction can modify climate model simulated precipitation changes without adverse effect on the ensemble mean, *Hydrol. Earth Syst. Sci.*, *18*, 915–925.
- Maurer, E. P., and H. G. Hidalgo (2008), Utility of daily vs. monthly large-scale climate data: An intercomparison of two statistical downscaling methods, *Hydrol. Earth Syst. Sci.*, *12*, 551–563.
- Maurer, E. P., A. W. Wood, J. C. Adam, D. P. Lettenmaier, and B. Nijssen (2002), A long-term hydrologically-based data set of land surface fluxes and states for the conterminous United States, *J. Clim.*, *15*(22), 3237–3251.
- McAdam, S. A. M., and T. J. Brodrigg (2015), The evolution of mechanisms driving the stomatal response to vapour pressure deficit, *Plant Physiol.*, *167*, 833–843.
- McDowell, N. G., and C. D. Allen (2015), Darcy's law predicts widespread forest mortality under climate warming, *Nat. Clim. Change*, *5*(7), 669–672.
- McDowell, N., et al. (2002), The relationship between tree height and leaf area: Sapwood area ratio, *Oecologia*, *132*(1), 12–20.
- Medlyn, B. E., et al. (2001), Stomatal conductance of forest species after long-term exposure to elevated CO₂ concentration: A synthesis, *New Phytol.*, *149*(2), 247–264.
- Medlyn, B. E., R. A. Duursma, D. Eamus, D. S. Ellsworth, I. C. Prentice, C. V. M. Barton, K. Y. Crous, P. De Angelis, M. Freeman, and L. Wingate (2011), Reconciling the optimal and empirical approaches to modelling stomatal conductance, *Global Change Biol.*, *17*(6), 2134–2144.
- Milly, P. C. D., and K. A. Dunne (2016), Potential evapotranspiration and continental drying, *Nat. Clim. Change*, *6*, 946–949, doi:10.1038/nclimate3046.
- Mitchell, T. D., T. R. Carter, P. D. Jones, M. Hulme, and M. G. New (2004), A comprehensive set of high-resolution grids of monthly climate for Europe and the globe: The observed record (1901–2000) and 16 scenarios (2001–2100), *Rep.*, 30 pp., Tyndall Centre for Climate Change Research, Univ. of East Anglia, Norwich, U. K.
- Monteith, J. L. (1965), Evaporation and environment, in *The State and Movement of Water in Living Organisms, Symposium of the Society of Experimental Biology*, vol. 19, edited by B. D. Fogg, pp. 205–234, Cambridge Univ. Press, Cambridge.
- Novick, K. A., et al. (2016), The increasing importance of atmospheric demand for ecosystem water and carbon fluxes, *Nat. Clim. Change*, *6*, 1023–1027.
- Novick, K., R. Oren, P. Stoy, J.-Y. Juang, M. Siqueira, and G. Katul (2009), The relationship between reference canopy conductance and simplified hydraulic architecture, *Adv. Water Resour.*, *32*(6), 809–819.
- Oren, R., J. S. Sperry, G. G. Katul, D. E. Pataki, B. E. Ewers, N. Phillips, and K. V. R. Schäfer (1999), Survey and synthesis of intra- and interspecific variation in stomatal sensitivity to vapour pressure deficit, *Plant Cell Environ.*, *22*(12), 1515–1526.
- Penman, H. L. (1948), Natural evaporation from open water, bare soil and grass, *Proc. R. Soc. London. A: Math. Phys. Eng. Sci.*, *193*(1032), 120–145.
- Piao, S., P. Friedlingstein, P. Ciais, L. Zhou, and A. Chen (2006), Effect of climate and CO₂ changes on the greening of the Northern Hemisphere over the past two decades, *Geophys. Res. Lett.*, *33*, L23402, doi:10.1029/2006GL028205.
- Pierce, D. W., D. R. Cayan, E. P. Maurer, J. T. Abatzoglou, and K. C. Hegewisch (2015), Improved Bias Correction Techniques for Hydrological Simulations of Climate Change, *J. Hydrometeorol.*, *16*(6), 2421–2442.
- Polade, S. D., A. Gershunov, D. R. Cayan, M. D. Dettinger, and D. W. Pierce (2013), Natural climate variability and teleconnections to precipitation over the Pacific-North American region in CMIP3 and CMIP5 models, *Geophys. Res. Lett.*, *40*, 2296–2301, doi:10.1002/grl.50491.
- Prein, A. F., G. J. Holland, R. M. Rasmussen, M. P. Clark, and M. R. Tye (2016), Running dry: The U.S. Southwest's drift into a drier climate state, *Geophys. Res. Lett.*, *43*, 1272–1279, doi:10.1002/2015GL066727.
- Puma, M. J., and B. I. Cook (2010), Effects of irrigation on global climate during the 20th century, *J. Geophys. Res.*, *115*, D16120, doi:10.1029/2010JD014122.
- Racherla P., D. Shindell, and G. Faluvegi (2012), The added value to global model projections of climate change by dynamical downscaling: A case study over the continental U.S. using the GISS-ModelE2 and WRF models, *J. Geophys. Res.*, *117*, D20118, doi:10.1029/2012JD018091.
- Rigden, A. J., and G. D. Salvucci (2016), Stomatal response to humidity and CO₂ implicated in recent decline in US evaporation, *Global Change Biol.*, Early View.
- Roderick, M. L., and G. D. Farquhar (2002), The cause of decreased pan evaporation over the past 50 years, *Science*, *298*(5597), 1410–1411.
- Roman, D. T., K. A. Novick, E. R. Brzostek, D. Dragoni, F. Rahman, and R. P. Phillips (2015), The role of isohydric and anisohydric species in determining ecosystem-scale response to severe drought, *Oecologia*, *179*(3), 641–654.
- Rupp, D. E., J. T. Abatzoglou, K. C. Hegewisch, and P. W. Mote (2013), Evaluation of CMIP5 20th century climate simulations for the Pacific Northwest USA, *J. Geophys. Res. Atmos.*, *118*, 10,906–10,884, doi:10.1002/jgrd.50843.
- Sacks, W. J., B. I. Cook, N. Buening, S. Levis, and J. H. Helkowski (2009), Effects of global irrigation on the near-surface climate, *Clim. Dyn.*, *33*, 159–175.
- Sanford, T., P. C. Frumhoff, A. Luers, and J. Gullede (2014), The climate policy narrative for a dangerously warming world, *Nat. Clim. Change*, *4*(3), 164–166.
- Sato, H., T. O. Kumagai, A. Takahashi, and G. G. Katul (2015), Effects of different representations of stomatal conductance response to humidity across the African continent under warmer CO₂-enriched climate conditions, *J. Geophys. Res. Biogeosciences*, *120*, 979–988, doi:10.1002/2014JG002838.
- Seager, R., A. Hooks, A. P. Williams, B. Cook, J. Nakamura, and N. Henderson (2015), Climatology, variability, and trends in the U.S. Vapor pressure deficit, an important fire-related meteorological quantity, *J. Appl. Meteorol. Climatol.*, *54*(6), 1121–1141.
- Sen, P. K. (1968), Estimates of the regression coefficient based on Kendall's Tau, *J. Am. Stat. Assoc.*, *63*(324), 1379–1389.
- Sheffield, J., and E. F. Wood (2008), Projected changes in drought occurrence under future global warming from multi-model, multi-scenario, IPCC AR4 simulations, *Clim. Dyn.*, *31*(1), 79–105.

- Sherwood, S., and Q. Fu (2014), A drier future?, *Science*, 343(6172), 737–739.
- Smith, K. W., S. C. Reed, C. C. Cleveland, A. P. Ballantyne, W. R. L. Anderegg, W. R. Wieder, Y. Y. Liu, and S. W. Running (2016), Large divergence of satellite and Earth system model estimates of global terrestrial CO₂ fertilization, *Nat. Clim. Change*, 6(3), 306–310.
- Sperry, J. S., Y. Wang, B. T. Wolfe, D. S. Mackay, W. R. Anderegg, N. G. McDowell, and W. T. Pockman (2016), Pragmatic hydraulic theory predicts stomatal responses to climatic water deficits, *New Phytol.*, 212, 577–589.
- Stoy, P., G. G. Katul, M. B. S. Siqueira, J. Y. Juang, K. A. Novick, H. R. McCarthy, A. C. Oishi, J. M. Uebelherr, H.-S. Kim, and R. Oren (2006), Separating the effects of climate and vegetation on evapotranspiration along a successional chronosequence in the southeastern U.S., *Global Change Biol.*, 12, 1–21.
- Theil, H. (1992), A rank-invariant method of linear and polynomial regression analysis, in *Henri Theil's Contributions to Economics and Econometrics: Econometric Theory and Methodology*, edited by B. Raj and J. Koerts, pp. 345–381, Springer, Dordrecht, Netherlands.
- van den Honert, T. H. (1948), Water transport in plants as a catenary process, *Discuss. Faraday Soc.*, 3, 146–153.
- Vose, R. S., D. R. Easterling, and B. Gleason (2005), Maximum and minimum temperature trends for the globe: An update through 2004, *Geophys. Res. Lett.*, 32, L23822, doi:10.1029/2005GL024379.
- Whitehead, D. (1998), Regulation of stomatal conductance and transpiration in forest canopies, *Tree Physiol.*, 18(8-9), 633–644.
- Willett, K. M., N. P. Gillett, P. D. Jones, and P. W. Thorne (2007), Attribution of observed surface humidity changes to human influence, *Nature*, 449(7163), 710–712.
- Williams, A. P., et al. (2013), Temperature as a potent driver of regional forest drought stress and tree mortality, *Nat. Clim. Change*, 3(3), 292–297.
- Williams, A. P., et al. (2014), Causes and implications of extreme atmospheric moisture demand during the record-breaking 2011 wildfire season in the southwestern United States, *J. Appl. Meteorol. Climatol.*, 53(12), 2671–2684.
- Williams, A. P., et al. (2015), Correlations between components of the water balance and burned area reveal new insights for predicting forest fire area in the southwest United States, *Int. J. Wildland Fire*, 24(1), 14–26.
- Yue, S., P. Pilon, and G. Cavadias (2002), Power of the Mann-Kendall and Spearman's rho tests for detecting monotonic trends in hydrological series, *J. Hydrol.*, 259, 254–271.
- Zhang, K., J. S. Kimball, R. R. Nemani, S. W. Running, Y. Hong, J. J. Gourley, and Z. Yu (2015), Vegetation greening and climate change promote multidecadal rises of global land evapotranspiration, *Sci. Rep.*, 5, doi:10.1038/srep15956.